

Simulated scanning tunneling microscopy images of few-layer-phosphorus capped by graphene and hexagonal boron nitride monolayers

Pablo Rivero,¹ Cedric M. Horvath¹, Zhen Zhu², Jie Guan², David Tománek^{2,*}, and Salvador Barraza-Lopez*

1. Department of Physics, University of Arkansas, Fayetteville, AR 72701, USA

2. Physics and Astronomy Department, Michigan State University, East Lansing, MI 48824, USA

(Dated: April 26, 2022)

Elemental phosphorous is believed to have several stable allotropes that are energetically nearly degenerate, but chemically reactive. To prevent chemical degradation under ambient conditions, these structures may be capped by monolayers of hexagonal boron nitride (*h*-BN) or graphene. We perform *ab initio* density functional calculations to simulate scanning tunneling microscopy (STM) images of different layered allotropes of phosphorus and study the effect of capping layers on these images. We find that protective monolayers of insulating *h*-BN allow to distinguish between the different structural phases of phosphorus underneath, even though the images are filtered through only nitrogen atoms that appear transparent. No such distinction is possible for phosphorus films capped by semimetallic graphene that masks the underlying structure. Our results suggest that the real-space imaging capability of STM is not hindered by selected capping layers that protect phosphorus surfaces.

PACS numbers: 68.37.Ef, 31.15.A-, 73.90.+f

I. INTRODUCTION

There has been an unprecedented interest in layered phosphorus allotropes as a new member of the family of two-dimensional (2D) materials [1, 2] in the post-graphene era. The interest has been triggered by reports that layered bulk black phosphorus[3–11] can be exfoliated mechanically, yielding few-layer phosphorene with a significant fundamental band gap and high carrier mobility[12–15] exceeding that of transition metal dichalcogenides (MX_2 's)[16]. Few-layer phosphorene bears promise for intriguing optoelectronics applications[17], since the fundamental band gap can be tuned by the number of layers and in-layer stretching or compression[12, 18–23]. But what truly sets phosphorene apart from other 2D systems is its polymorphism: Besides the well-studied black phosphorus allotrope, energetically near-degenerate alternate structures have been postulated including blue phosphorus, γ -P, δ -P and their combination in one layer[24–32]. Identifying and discriminating between these structures requires a tool capable of probing structures in real space with sub-nanometer resolution. Scanning Tunneling Microscopy (STM) is such an ideal tool, but requires chemically stable samples.

Even though phosphorene is known to degrade under ambient conditions,[14, 33, 34] significant progress has been achieved in its stabilization by passivating the exposed surface.[35] In the initial transport studies this passivation has been achieved by a thick PMMA coating[12–15] that, of course, precludes an STM study of the underlying structure. Besides PMMA, however, also monolayers of graphene and hexagonal boron nitride (*h*-BN)[36–

38] have proven effective in this sense, constituting the thinnest “*galvanizing agents*.” Also capping by graphene or *h*-BN monolayers has been shown to protect phosphorene from degradation.[34, 39] Similar to graphene, *h*-BN is a chemically inert material that can be exfoliated from bulk material by mechanical transfer [40–43], or can be synthesized by chemical vapor deposition[44]. Unlike in semimetallic graphene, the observed fundamental band gap close to 6 eV is very large[45].

Even though a structure may be capped by a passivating graphene monolayer, it has been established that the underlying structure can be revealed by STM studies in a process called “electronic transparency.”[46] The objective of this computational study is to establish whether different phosphorene allotropes can also be distinguished in STM studies when covered by a monolayer of graphene or *h*-BN. If so, then STM may also be able to reveal line defects including disclinations[47] and grain boundaries separating different phases in the underlying phosphorene layer[48]. The nature and concentration of defects is critical for the stability of phosphorene since defects act as nucleation sites in the material degradation process.

II. METHODS

Calculations have been carried out using the SIESTA *ab initio* simulation package[49] with a cut-off energy of 300 Ry. The optB88-vdW local exchange functional[50] has been used to describe van der Waals interactions. Norm-conserving Troullier-Martins pseudopotentials[51] and a double- ζ basis including polarization orbitals were employed in calculations. Structural relaxations were performed using the conjugate gradient method until the atomic forces were below 0.04 eV/Å. The electron densities were integrated over dense k-point meshes using an in-house program, and visualized with the Denchar

*Electronic address: tomanek@pa.msu.edu, sbarraza@uark.edu

program.

III. RESULTS AND DISCUSSION

We have used *ab initio* density functional theory calculations, specified in the Methods section, to determine the equilibrium geometry and electronic band structure of thin slabs of multi-layer phosphorene capped on both sides with passivating graphene or hexagonal boron nitride monolayers. We considered thin slabs of black phosphorus (black P), blue phosphorus (blue P), δ phosphorus (δ -P) and γ phosphorus (γ -P).[24, 25, 52–54] The optimum geometries and electronic band structures of these systems are shown in Fig. 1.

A. Equilibrium geometry and stability of capped phosphorus slabs

For the sake of a simple comparison, we have considered thin slabs containing 5 phosphorene layers in their optimum geometry, with no relative in-plane displacements nor rotational faults. The fundamental band gap and optimum inter-layer separation l , defined in Fig. 1, approach their limiting bulk values at this thickness already.[25].

Keeping the optimum unit cell size of the 2D phosphorene slab, we capped the slabs by a graphene or a *h*-BN monolayer on both sides to suppress spurious dipole effects. The equilibrium geometry of all structures considered here is reproduced in Fig. 1. Only two layers of the 5-layer phosphorene slabs are shown in the structural side views. The coloring of atomic species in *h*-BN covered P is as follows: Atoms in the top P layer are shown in white and N atoms in light blue. All other P atoms are shown in brown, B atoms in orange and C atoms in red. As we will show later on, the P atoms in the top layer and the N atoms play an important role in the STM images of phosphorene covered by BN. The unit cells are shown in the left sub-panels, and the Brillouin zones are shown as insets in the band structure plots. Black phosphorene, δ -P and γ -P have rectangular unit cells and Brillouin zones,[25] whereas blue phosphorene has a hexagonal unit cell and Brillouin zone reminiscent of graphene[24].

The size of the supercells, listed in Table I, ranges from 92 to 184 atoms. The average distance d between the top-most P atoms (shown in white in Fig. 1) and the *h*-BN or graphene capping layer is listed in Table II and ranges from 3.55 Å in γ -P to 3.90 Å in δ -P. Since the equilibrium lattice constant of *h*-BN and graphene monolayers differs by as much as 7% from that of the phosphorus slabs, the capping layers have been stretched or compressed to enforce epitaxy. In the δ -P slab, the *h*-BN overlayer shows an energetic preference for a wavy structure[55], shown in Fig. 1c, over a planar compressed structure, displaying

a pattern reminiscent of the observed structure in slabs of phosphorus IV[56].

Next we investigated the adhesion of the capping layer on the phosphorus slab. We defined the adhesion energy E_{ad} by

$$E_{ad} = (1/2)[E_{tot}(\text{capped P slab}) - 2E_{tot}(\text{capping layer}) - E_{tot}(\text{P slab})]. \quad (1)$$

Here, $E_{tot}(\text{capped P slab})$ is the total energy of the P slab capped by either *h*-BN or graphene at both exposed surfaces, $E_{tot}(\text{P slab})$ is the total energy of the isolated P slab, and $E_{tot}(\text{capping layer})$ is the energy of a single monolayer of *h*-BN or graphene. Negative values indicate energy gain, and the factor 1/2 takes care of the fact that the slab is capped at both sides. We find it useful to divide the adsorption energy by the interface area A and list the values of E_{ad}/A in Table II. *h*-BN/black P turns out to be the most stable capped system, with an energy gain upon adhesion of 21.60 meV/Å². *h*-BN/ δ -P has the weakest adhesion energy (19.49 meV/Å²), which is caused by a larger average separation between *h*-BN and the wavy phosphorene layer, seen in the left panel of Fig. 1c. We discuss the relative location of *h*-BN and phosphorus electron bands next.

B. Electronic structure of capped phosphorus slabs

To simplify the interpretation of our electronic structure results in Fig. 1, we distinguished states associated predominantly with P slabs, shown in gold, from states associated predominantly with the capping layers, shown in red. The Fermi level of the *h*-BN capped phosphorene slab is set at $E_F = 0$ eV. The DFT value of the fundamental band gap of an isolated *h*-BN monolayer is 4.5 eV. The fact that the Fermi level of the capping layer alone lies above the Fermi level of the *h*-BN/P system indicates *p*-doping of the *h*-BN monolayer. This occurs as the π -electron clouds of *h*-BN and phosphorene overlap, causing electron transfer from *h*-BN to P. A similar behavior has been seen in weakly adsorbed carbon nanotubes on Si.[57] We determine a gap of 4.5 eV for *h*-BN, a band gap of 0.44 eV in black P, 1.03 eV in blue P, and 0.21 eV in δ -P slabs, and find the γ -P slab to be metallic[25], as seen in Fig. 1. These gaps are further emphasized in the total density of states (DOS) plots shown to the right of each band structure plot. The alignment of the *h*-BN electron bands with respect to those of the phosphorene slabs depends further on the relative distance d between *h*-BN and the phosphorene slab. Presence of structural defects or chemical contamination leads to doping, which causes additional band shifts. These effects are addressed next.

When an STM samples a layered material, it pushes/pulls it away from its equilibrium atomistic configuration as it attempts to establish a feedback current[46]. This effect is studied here in detail: We

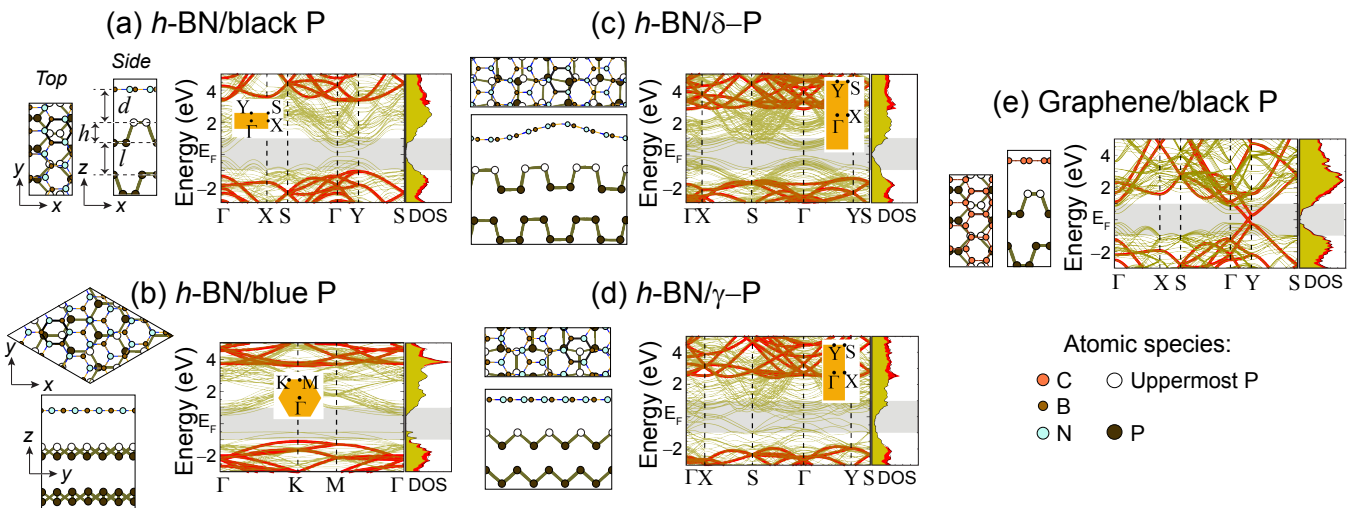


FIG. 1: Atomistic structure and electronic properties of five-layer phosphorene slabs capped with hexagonal boron nitride (*h*-BN, subplots a-d) and graphene (subplot e) monolayers. Equilibrium geometry is in the left sub-panels, and Brillouin zones are reproduced as insets in the band structure plots. P atoms in the top layer, which contribute most to STM images, are colored in white. The grey shaded band around E_F indicates the energy range probed by STM. Electronic states associated with the *h*-BN or graphene capping layers are shown in red and bands associated with phosphorus in gold in the band structure and the total density of states (DOS) plots in the right sub-panels.

register rigid band shifts of the *h*-BN with magnitudes -0.166 eV, -0.075 eV, $+0.045$ eV, and $+0.075$ eV with respect to the band alignment shown in Fig. 1a, as the *h*-BN monolayer is located -0.4 Å, -0.2 Å, $+0.2$ Å, or $+0.4$ Å away from the black P slab with respect to its equilibrium atomistic configuration on the structural model in Fig. 1a, respectively. This indicates that the electron cloud on *h*-BN finds a larger Coulomb repulsion when it approaches the phosphorene slab. This mechanical effect is similar to that produced by doping: When a phosphorus atom is replaced by a carbon atom, the slab becomes *p*-doped and the *h*-BN bands, shown in bold red in Fig. 1a, shift down by 0.517 eV. There is a significant energy window with zero density even when these inevitable energy shifts are considered: *h*-BN may thus appear transparent under STM measurements. While protecting phosphorene, it permits the identification of atomistic features of the phosphorene structure, as will be discussed in the following.

C. Simulation of STM images

It is well established that STM images can be simulated by *ab initio* density functional calculations.[58] Applying a small bias voltage V_{bias} between the sample and the STM tip yields a tunneling current, whose density $j(\mathbf{r})$ can be obtained from a simple extension[59] of the expression derived by Tersoff and Hamann,[60, 61]

$$j(\mathbf{r}, V_{bias}) \propto \rho_{STM}(\mathbf{r}, V_{bias}), \quad (2)$$

where

$$\rho_{STM}(\mathbf{r}, V_{bias}) = \int_{E_F - eV_{bias}}^{E_F} dE \rho(\mathbf{r}, E) \quad (3)$$

and

$$\rho(\mathbf{r}, E) = \sum_{n, \mathbf{k}} |\psi_{n\mathbf{k}}(\mathbf{r})|^2 \delta(E_{n, \mathbf{k}} - E). \quad (4)$$

Here, $\rho(\mathbf{r}, E)$ is the local density of states at the center of curvature of the tip at \mathbf{r} and $\psi_{n\mathbf{k}}(\mathbf{r})$ are the electron eigenstates of the unperturbed surface at energy $E_{n, \mathbf{k}}$. These eigenstates are commonly represented by Kohn-Sham eigenstates obtained using density functional theory. The implied assumptions[59–61] are that the relevant tip states are well described by *s* waves with a constant density of states. Furthermore, the tunneling matrix element is considered to be independent of the lateral tip position for a constant tip-to-surface distance and also independent of the bias voltage V_{bias} in the narrow (but nonzero) energy region $[E_F - eV_{bias}, E_F]$. Whereas Equation 3 describes tunneling from occupied states of the sample to the tip, an obvious change of this expression can describe tunneling from the tip to unoccupied states in the energy range $[E_F, E_F + e|V_{bias}|]$. This latter configuration is referred to as reverse bias and described by a negative bias voltage.

D. Simulated STM images of bare few-layer phosphorene slabs

Simulated STM images of bare few-layer phosphorene slabs, representing the charge density $\rho_{STM}(\mathbf{r}, V_{bias})$,

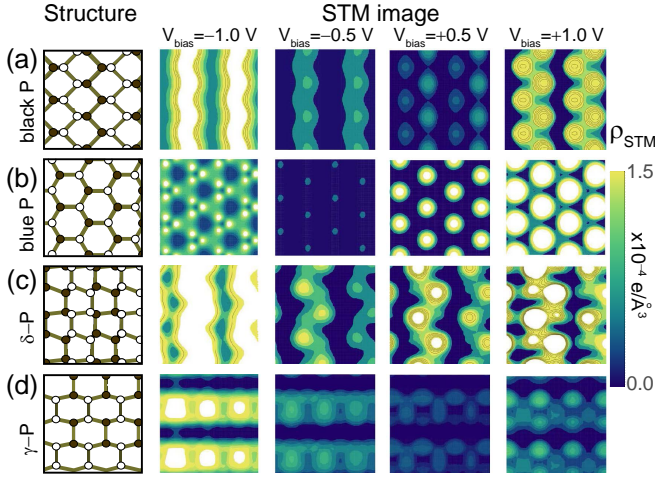


FIG. 2: Simulated STM images of a $10 \text{ \AA} \times 10 \text{ \AA}$ area of bare (a) black phosphorene, (b) blue-phosphorene, (c) δ -P and (d) γ -P slabs. Presented is ρ_{STM} at constant height, corresponding to the current imaging mode, at different values of the bias voltage V_{bias} . For the sake of simple comparison, the geometry of the topmost two layers of the slabs is reproduced to scale in the left panels, with topmost atoms shown in white. Streaks seen on black phosphorene, δ -P and γ -P reflect their “ridged” atomistic structure, also highlighted in the structural models. The different threefold symmetry of blue phosphorene with a triangular sublattice, associated with the white-colored P atoms in the topmost layer, is clearly reflected in the STM images in (b).

given by Equation 3, at various bias voltages V_{bias} are presented in Fig. 2. For better interpretation of the images, we reproduced the atomic arrangement in the topmost layers of the slab in the left panels. Visual comparison of the structures and the STM images reveals that the highest values of ρ_{STM} correlate well with the location of the topmost P atoms, which are shown in white in the structural depiction. Underlying all STM images is a dense k -point mesh used in Equation 4 for the charge density integration. The STM image is represented by ρ_{STM} scanned within a plane at the distance $d = 2.3 \text{ \AA}$ from the closest phosphorus atoms shown in white. For the sake of simple comparison, we keep the scan area and the color bars the same in Figs. 2 to 4.

An antibonding-like feature is visible by the spatial distribution localized over P atoms at forward bias V_{bias} on black P (Fig. 2a). On the other hand, a bonding-like feature is reproduced under a negative bias as the electronic density is larger at bonds between pairs of P atoms. In blue phosphorus (Fig. 2b) a triangular shape of the electronic density is seen under forward bias due to the electronic density coming only from the upper P atoms. The images under a reverse bias $V_{bias} = -1V$ show a decorated triangular lattice displaying three bright small circles around each uppermost (white) P atom. The higher intensity for $V_{bias} > 0$ correlates with the rather flat valence band seen on Fig. 1b (the reader must divide the energy scale in Fig. 1 by $-|e|$ to obtain V_{bias} on Figs. 2

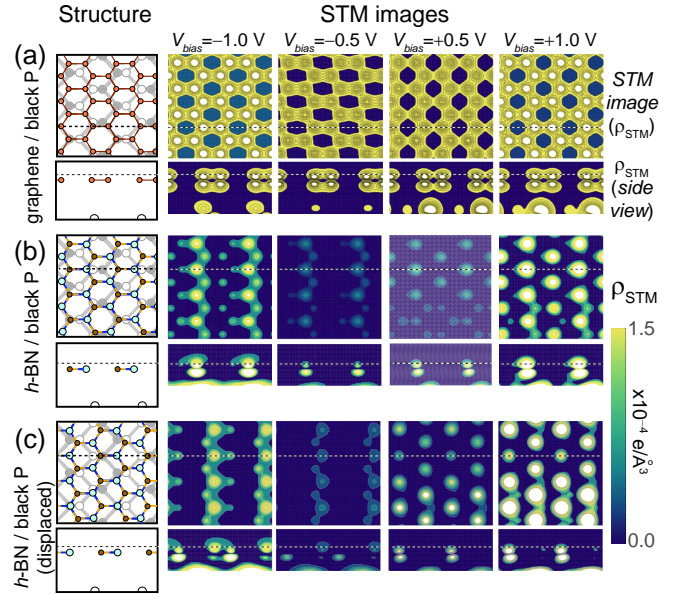


FIG. 3: Simulated STM images of a $10 \text{ \AA} \times 10 \text{ \AA}$ area of a black phosphorene slab capped by a monolayer of (a) graphene, (b) h -BN and (c) a horizontally displaced h -BN monolayer. Presented is ρ_{STM} at constant height, corresponding to the current imaging mode, at different values of the bias voltage V_{bias} . The lower sub-panels represent ρ_{STM} in a plane normal to the surface. For the sake of simple comparison, the geometry of the topmost layers of the slabs is reproduced to scale in the left panels, with topmost P atoms shown in white. The ridged structure of black P, which is clearly visible in Fig. 2a at $V_{bias} = -1.0 V$, is completely obscured by a graphene layer in (a), but is visible underneath an h -BN layer in (b) and (c).

to 4).

Two vertical trenches can be seen in δ -P (Fig. 2c) for forward and reverse biases, but the shape of these trenches is different depending on bias direction: The electronic density ρ_{STM} is localized onto the upper P atoms for positive V_{bias} , and it appears more distributed over bonds under reverse biases; this is particularly evident for $V_{bias} = -1V$. The spatial density acquired above the γ -P slab also exhibits two horizontal trenches under negative bias in a bonding-like fashion as the charge is distributed away from atoms and into covalent bonds (Fig. 2d). Due to the antibonding-like distribution, these electronic density trenches can be seen localized over the P atoms when $V_{bias} > 0 V$.

Clearly, different structural phases can be distinguished with an STM. Next we will study if these structures remain distinguishable by STM when covered by a capping monolayer.

E. Simulated STM images of few-layer phosphorus slabs capped by graphene or h -BN

Simulated STM images of few-layer black phosphorene slabs capped by graphene or h -BN are presented in Fig. 3.

In the current imaging mode, the STM current is represented by the charge density $\rho_{STM}(\mathbf{r}, V_{bias})$, given by Equation 3. We present ρ_{STM} at various bias voltages V_{bias} in a plane parallel to the surface, indicated by a dashed horizontal line in the structural image in side view. We also present ρ_{STM} in a plane normal to the surface, indicated by a dashed horizontal line in the structural image in top view. These images allow us to judge, whether the structure of a phosphorene slab may be distinguished underneath a capping monolayer of graphene or *h*-BN.

In the case of III-V semiconductors, a capping monolayer of graphene, when pushed by the STM tip to close proximity of the substrate, was found to not to conceal the atomic structure of the substrate. As seen in Fig. 3a, this is clearly not the case for black phosphorene covered by graphene. Independent of the bias voltage, the simulated STM images are dominated by the structure of the graphene overlayer. The significantly larger density of graphene states in the scanning plane efficiently masks the ridged structure of black phosphorene, which is most clearly visible in the STM image of the bare surface at $V_{bias} = -1.0$ V in Fig. 2a. Also, the side view images – cut along a carbon covalent bond – show a symmetric distribution of the electronic density of the π -bond among pairs of carbon atoms. As we will discuss in the following, this symmetry will not be preserved by *h*-BN, which will have direct consequences for the STM images obtained using *h*-BN as the capping monolayer.

In contrast to the semimetallic graphene, *h*-BN as a protective capping layer does not contribute states within the energy range probed by STM due to its large fundamental band gap. The fact that the STM images in Fig. 3b and 3c contain information indicates that the *h*-BN layer appears, to some degree, transparent to the STM,[46] allowing to discriminate between different phosphorene phases[26]. As a result of small but finite hybridization, the white/yellow streaks in STM images in Fig. 2a at $V_{bias} = -1.0$ V highlighting the ridges on a bare black phosphorene surface become also visible underneath an *h*-BN layer in Fig. 3b and 3c. To further understand the differences between Figs. 2a and 3b, caused by the presence of the capping *h*-BN layer, we compare the distribution of ρ_{STM} in a plane normal to the surface in the following.

Whereas the *h*-BN monolayer does not contribute any states to the STM image in Fig. 3b, the charge distribution of the phosphorene slab appears to be filtered non-uniformly through the capping layer. Careful comparison between the side views of the structural model and the density plots reveals that charge density of phosphorene underneath is filtered predominantly through N atoms of the capping layer, which are shown in light blue. The reason for this finding is the ionic character of BN. The deeper electronic potential on N not only causes an electron transfer from B atoms, but also extends the range of phosphorene states to above the *h*-BN layer, where they are probed by the STM.

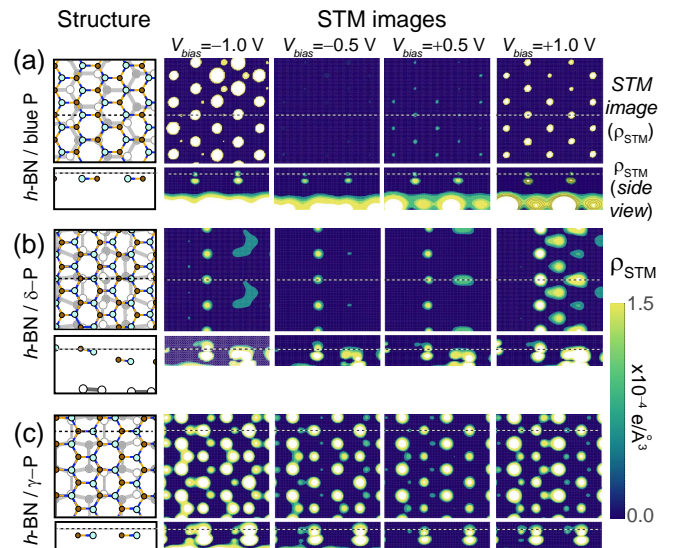


FIG. 4: Simulated STM images of a $10 \text{ \AA} \times 10 \text{ \AA}$ area of a (a) blue phosphorene, (b) δ -P and (c) γ -P slab capped with an *h*-BN monolayer. Presented is ρ_{STM} at constant height, corresponding to the current imaging mode, at different values of the bias voltage V_{bias} . The lower sub-panels represent ρ_{STM} in a plane normal to the surface. For the sake of simple comparison, the geometry of the topmost layers of the slabs is reproduced to scale in the left panels, with topmost P atoms shown in white.

Even though the adhesion of the *h*-BN layer on the phosphorene substrate is substantial according to Table II, contact with the STM tip may shift the capping layer horizontally. In the following, we discuss the effect of such a horizontal displacement on the STM image. Figs. 3b and 3c both represent a black P slab covered by *h*-BN; the capping layer in 3c has been shifted from its position in 3b. This displacement can be visualized most easily in the side view of the atomic structure, in a plane normal to the surface. As seen at the top of the left panels in Figures 3b and 3c, this plane contains two P atoms in the topmost P layer. At the bottom of the left panels of these sub-figures, we can see the effect of a horizontal displacement by 1.44 \AA . One of the P atoms, which was underneath an N atom in Fig. 3b, appears underneath a B atom in 3c. Even though this displacement represents the worst-case scenario of switching from P-N registry to P-B registry, the STM images in Figs. 3b and 3c are rather similar at all bias voltages, indicating image stability with respect to a displacement of the capping layer. In particular, the ridged structure, which dominated the image of the bare surface in Fig. 2a, is pronounced in both images.

To judge, whether the different allotropes can be distinguished underneath an *h*-BN monolayer, we have simulated STM images of blue P, δ -P and γ -P. We find these images, presented in Fig. 4, to be all different, and to also differ from those of black P in Fig. 3b and 3c. In comparison to black P with a rectangular unit cell, Fig. 4a

clearly reveals the honeycomb lattice of the underlying blue phosphorene. Similarly, ρ_{STM} of a capped δ -P slab in Fig. 4b displays two vertical stripes at locations above N atoms at negative bias values, in close agreement with Fig. 2c. Due to its wavy morphology, the capping layer binds least to the substrate and is most likely to be displaced by an STM tip during scanning. The STM images of a capped γ -P slab, shown in Fig. 4c, display similar ridges as seen in the bare γ -P slab, shown in Fig. 2d.

The main message of our simulated STM images, presented in Figs. 2-4, is that STM is capable of distinguishing between different phases of layered phosphorus underneath a passivating hexagonal boron nitride monolayer.

IV. CONCLUSIONS

In summary, we have studied the electronic structure and simulated scanning tunnel microscopy of few-layer

phosphorus allotropes capped by *h*-BN and graphene monolayers using density functional theory with vdW corrections. Our results indicate that capping by *h*-BN does permit identifying phosphorus phases underneath. Due to the vanishing band gap of graphene, the charge density of capping graphene monolayers masks the structure underneath, making this structure unsuitable to discriminate between different phosphorene allotropes. These results may assist the nascent experimental searches for different structural phases of layered phosphorus.

We thank NSF-XSEDE (Grant TG-PHY090002; TACC's *Stampede*) and Arkansas (*Razor II*) for computational support. P.R. and S.B.L. acknowledge funding from the Arkansas Biosciences Institute. Z.Z., J.G. and D.T. acknowledge support by the National Science Foundation Cooperative Agreement No. EEC-0832785, titled "NSEC: Center for High-Rate Nanomanufacturing".

-
- [1] K. S. Novoselov, D. Jiang, F. Schedin, T. J. Booth, V. V. Khotkevich, S. Morozov, and A. Geim, Proc. Natl. Acad. Sci. (USA) **102**, 10451 (2005).
 - [2] S. Z. Butler, S. M. Hollen, L. Cao, Y. Cui, J. A. Gupta, H. R. Gutiérrez, T. F. Heinz, S. S. Hong, J. Huang, A. F. Ismach, et al., ACS Nano **7**, 2898 (2013).
 - [3] P. W. Bridgman, J. Am. Chem. Soc. **36**, 1344 (1914), <http://dx.doi.org/10.1021/ja02184a002>, URL <http://dx.doi.org/10.1021/ja02184a002>.
 - [4] R. W. Keyes, Phys. Rev. **92**, 580 (1953).
 - [5] R. C. Ellis and D. M. Warschauer, J. Electrochem. Soc. **109**, C207 (1962).
 - [6] J. C. Jamieson, Science **139**, 1291 (1963).
 - [7] D. Schiferl, Phys. Rev. B **19**, 806 (1979).
 - [8] H. Asahina, K. Shindo, and A. Morita, J. Phys. Soc. Jap. **51**, 1193 (1982).
 - [9] H. Kawamura, I. Shirovani, and K. Tachikawa, Solid State Comm. **49**, 879 (1984).
 - [10] Y. Akahama, H. Kawamura, S. Carlson, T. Le Bihan, and D. Häusermann, Phys. Rev. B **61**, 3139 (2000).
 - [11] G. Monaco, S. Falconi, W. A. Crichton, and M. Mezouar, Phys. Rev. Lett. **90**, 255701 (2003).
 - [12] H. Liu, A. T. Neal, Z. Zhu, Z. Luo, X. Xu, D. Tománek, and P. D. Ye, ACS Nano **8**, 4033 (2014).
 - [13] L. Li, Y. Yu, G. J. Ye, Q. Ge, X. Ou, H. Wu, D. Feng, X. H. Chen, and Y. Zhang, Nature Nanotech. **9**, 372 (2014).
 - [14] S. P. Koenig, R. A. Doganov, H. Schmidt, A. H. Castro Neto, and B. Özyilmaz, Appl. Phys. Lett. **104**, 103106 (2014).
 - [15] M. Buscema, D. J. Groenendijk, S. I. Blanter, G. A. Steele, H. S. J. van der Zant, and A. Castellanos-Gomez, Nano Lett. **14**, 3347 (2014).
 - [16] V. Tran, R. Soklaski, Y. Liang, and L. Yang, Phys. Rev. B **89**, 235319 (2014).
 - [17] H. O. H. Churchill and P. Jarillo-Herrero, Nature Nanotech. **9**, 330 (2014).
 - [18] R. Fei and L. Yang, Nano Lett. **14**, 2884 (2014).
 - [19] A. S. Rodin, A. Carvalho, and A. H. Castro Neto, Phys. Rev. Lett. **112**, 176801 (2014).
 - [20] A. N. Rudenko and M. I. Katsnelson, Phys. Rev. B **89**, 201408 (2014).
 - [21] Q. Wei and X. Peng, Appl. Phys. Lett. **104**, 251915 (2014).
 - [22] J.-W. Jiang and H. S. Park, Nature Comm. **5**, 4727 (2014).
 - [23] X. Peng, Q. Wei, and A. Copple, Phys. Rev. B **90**, 085402 (2014).
 - [24] Z. Zhu and D. Tománek, Phys. Rev. Lett. **112**, 176802 (2014).
 - [25] J. Guan, Z. Zhu, and D. Tománek, Phys. Rev. Lett. **113**, 046804 (2014).
 - [26] J. Guan, Z. Zhu, and D. Tománek, ACS Nano p. Article ASAP. 10.1021/nn5059248 (2014), URL <http://dx.doi.org/10.1021/nn5059248>.
 - [27] J. Guan, Z. Zhu, and D. Tománek, Phys. Rev. Lett. **113**, 226801 (2014), URL <http://link.aps.org/doi/10.1103/PhysRevLett.113.226801>.
 - [28] S. Bocker and M. Haser, Z. Anorg. Allg. Chem. **621**, 258 (1995).
 - [29] G. Seifert and E. Hernandez, Chem. Phys. Lett. **318**, 355 (2000).
 - [30] A. J. Karttunen, M. Linnolahti, and T. A. Pakkanen, Chem. Phys. Phys. Chem. **9**, 2550 (2008).
 - [31] S. E. Boulfelfel, G. Seifert, Y. Grin, and S. Leoni, Phys. Rev. B **85**, 014110 (2012).
 - [32] X. Han, H. M. Stewart, S. A. Shevlin, C. R. A. Catlow, and Z. X. Guo, Nano Lett. **14**, 4607 (2014).
 - [33] A. Castellanos-Gomez, L. Vicarelli, E. Prada, J. O. Island, K. L. Narasimha-Acharya, S. I. Blanter, D. J. Groenendijk, M. Buscema, G. A. Steele, J. V. Alvarez, et al., 2D Materials **1**, 025001 (2014).
 - [34] J. D. Wood, S. A. Wells, D. Jariwala, K.-S. Chen, E. Cho, V. K. Sangwan, X. Liu, L. J. Lauhon, T. J. Marks, and M. C. Hersam, Nano Lett. p. Article ASAP. 10.1021/nl5032293 (2014), pMID: 25380142, <http://dx.doi.org/10.1021/nl5032293>, URL <http://dx.doi.org/10.1021/nl5032293>.

- doi.org/10.1021/nl5032293.
- [35] D. Tománek, *Mater. Express* **4**, 545 (2014).
- [36] J. Shin, K. Park, W.-H. Ryu, J.-W. Jung, and I.-D. Kim, *Nanoscale* **6**, 12718 (2014).
- [37] S. Chen, L. Brown, M. Levendorf, W. Cai, S.-Y. Ju, J. Edgeworth, X. Li, C. W. Magnuson, A. Velamakanni, R. D. Piner, et al., *ACS Nano* **5**, 1321 (2011).
- [38] T. Coan, G. S. Barroso, G. Motz, A. Bolzán, and R. A. F. Machado, *Mater. Res.* **16**, 1366 (2013).
- [39] N. Gillgren, D. Wickramaratne, Y. Shi, T. Espiritu, J. Yang, J. Hu, J. Wei, X. Liu, Z. Mao, K. Watanabe, et al. (2014), preprint, <http://arxiv.org/abs/1412.0717>.
- [40] C. R. Dean, A. F. Young, I. Meric, C. Lee, L. Wang, S. Sorgenfrei, K. Watanabe, T. Taniguchi, P. Kim, K. L. Shepard, et al., *Nat. Nanotechnol.* **5**, 722 (2010).
- [41] D. Pacilé, J. C. Meyer, C. O. Girit, and A. Zettl, *Appl. Phys. Lett.* **92**, 133107 (2008).
- [42] C. G. Lee, Q. Li, W. Kalb, X. Liu, H. Berger, R. W. Carpick, and J. Hone, *Science* **328**, 76 (2010).
- [43] C. R. Dean, A. F. Young, I. Meric, C. Lee, L. Wang, S. Sorgenfrei, K. Watanabe, T. Taniguchi, P. Kim, K. L. Shepard, et al., *Nat. Mater.* **5**, 722 (2010).
- [44] K. K. Kim, A. Hsu, X. Jia, S. M. Kim, Y. Shi, M. Hofmann, D. Nezich, J. F. Rodriguez-Nieva, M. Dresselhaus, T. Palacios, et al., *Nano Letters* **12**, 161 (2012).
- [45] K. Watanabe, T. Taniguchi, and H. Kanda, *Nat. Mater.* **3**, 404 (2004).
- [46] K. T. He, J. C. Koepke, S. Barraza-Lopez, and J. W. Lyding, *Nano Lett.* **10**, 3446 (2010).
- [47] Y. Liu, F. Xu, Z. Zhang, E. S. Penev, and B. I. Yakobson, *Nano Lett.* p. Article ASAP. 10.1021/nl5021393 (2014).
- [48] T. Höltzl, T. Veszprémi, and M. T. Nguyen, *C. R. Chemie* **13**, 1173 (2010).
- [49] E. Artacho, E. Anglada, O. Dieguez, J. D. Gale, A. García, J. Junquera, R. M. Martin, P. Ordejón, J. M. Pruneda, D. Sánchez-Portal, et al., *J. Phys. Cond. Mat.* **20**, 064208 (2008).
- [50] J. Klimes, D. R. Bowler, and A. Michaelides, *J. Phys. Condens. Matter* **22**, 022201 (2010).
- [51] N. Troullier and J. L. Martins, *Phys. Rev. B* **43**, 1993 (1991).
- [52] Y. Du, C. Ouyang, S. Shi, and M. Lei, *J. Appl. Phys.* **107**, 093718 (2010).
- [53] Ø. Prytz and E. Flage-Larsen, *J. Phys.: Condens. Matter* **22**, 015502 (2010).
- [54] S. Appalakondaiah, G. Vaitheeswaran, S. Lebégue, N. E. Christensen, and A. Svane, *Phys. Rev. B* **86**, 035105 (2012).
- [55] C. Tayran, Z. Zhu, M. Baldoni, D. Selli, G. Seifert, and D. Tománek, *Phys. Rev. Lett.* **110**, 176805 (2013), URL <http://link.aps.org/doi/10.1103/PhysRevLett.110.176805>.
- [56] H. Fujihisa, Y. Akahama, H. Kawamura, Y. Ohishi, Y. Gotoh, H. Yamawaki, M. Sakashita, S. Takeya, and K. Honda, *Phys. Rev. Lett.* **98**, 175501 (2007).
- [57] S. Barraza-Lopez, P. M. Albrecht, N. A. Romero, and K. Hess, *J. Appl. Phys.* **100**, 124304 (2006).
- [58] D. Tomanek and S. G. Louie, *Phys. Rev. B* **37**, 8327 (1988).
- [59] A. Selloni, P. Carnevali, E. Tosatti, and C. Chen, *Phys. Rev. B* **31**, 2602 (1985), URL <http://link.aps.org/doi/10.1103/PhysRevB.31.2602>.
- [60] J. Tersoff and D. Hamann, *Phys. Rev. Lett.* **50**, 1998 (1983), URL <http://link.aps.org/doi/10.1103/PhysRevLett.50.1998>.
- [61] J. Tersoff and D. Hamann, *Phys. Rev. B* **31**, 805 (1985), URL <http://link.aps.org/doi/10.1103/PhysRevB.31.805>.

TABLE I: Cell parameters and number of atoms per unit cell in phosphorus allotropes capped by graphene or *h*-BN monolayers. The lattice constants are $a_g = 2.49$ Å for graphene and $a_{BN} = 2.52$ Å for hexagonal boron nitride.

	black P		blue P	δ -P		γ -P	
	a	b	a	a	b	a	b
Cell parameters (Å)	4.58	10.05	9.97	16.51	5.43	13.60	5.35
Supercell size	1×3		3×3	3×1		4×1	
Total number of atoms	92		154	184		128	
Number of P atoms	60		90	120		80	

TABLE II: Structural information and adhesion energy E_{ad} of five-layer phosphorene slabs capped by *h*-BN or graphene. As defined in Fig. 1, the average distance between the closest P atoms (shown in white in the structural models) and the *h*-BN or graphene monolayer is d , the average thickness of the P layer is h , and the average interlayer separation in the P slab is l . E_{ad}/A is the adsorption energy E_{ad} of the capping layer on the phosphorus substrate, defined in Equation 1, divided by the area A .

	<i>h</i> -BN/black P	<i>h</i> -BN/blue P	<i>h</i> -BN/ δ -P	<i>h</i> -BN/ γ -P	graphene/black P
d (Å)	3.68	3.75	3.89	3.55	3.56
h (Å)	2.19	1.27	2.24	1.61	2.19
l (Å)	3.58	3.68	3.33	2.40	3.42
E_{ad}/A (meV/Å ²)	-21.60	-20.26	-19.49	-20.62	-20.38